# Test of Universal Rise of Hadronic Total Cross Sections based on $\pi p$, $Kp$ and $\bar{p}p, pp$ Scatterings

Muneyuki Ishida*

*Department of Physics, School of Science and Engineering,*

*Meisei University, Hino, Tokyo 191-8506, Japan*

Keiji Igi

*Theoretical Physics Laboratory, RIKEN, Wako, Saitama 351-0198, Japan*

(Dated: April 26, 2009)

## Abstract

Recently there are several evidences of the hadronic total cross section $\sigma_{\rm tot}$ to be proportional to $B\ \log^2 s$ consistent with the Froissart unitarity bound. The COMPETE collaborations have further assumed $\sigma_{\rm tot} \simeq B\ \log^2(s/s_0) + Z$ to extend its universal rise with the common value of $B$ and $s_0$ for all hadronic scatterings to reduce the number of adjustable parameters. The coefficient $B$ was suggested to be universal in the arguments of colour glass condensate (CGC) of QCD in recent years. There has been, however, no rigorous proof yet based only on QCD. We attempt to investigate the value of $B$ for $\pi^{\mp}p$, $K^{\mp}p$ and $\bar{p}p, pp$ scatterings respectively through the search for the simultaneous best fit to the experimental $\sigma_{\rm tot}$ and $\rho$ ratios at high energies. The $\sigma_{\rm tot}$ at the resonance and intermediate energy regions has also been exploited as a duality constraint based on the special form of finite-energy sum rule(FESR). We estimate the values of $B$, $s_0$ and $Z$ individually for $\pi^{\mp}p$, $K^{\mp}p$ and $\bar{p}p, pp$ scatterings without using the universality hypothesis. It turs out that the values of $B$ are mutually consistent within one standard deviation. It has to be stressed that we cannot obtain such a definite conclusion without the duality constraint. It is also interesting to note that the values of $Z$ for $\pi p$, $Kp$ and $\bar{p}(p)p$ approximately satisfy the ratio $2:2:3$ predicted by the quark model. The obtained value of $B$ for $\bar{p}(p)p$ is $B_{pp} = 0.280 \pm 0.015$mb, which predicts $\sigma_{\rm tot}^{pp} = 108.0 \pm 1.9mb$ and $\rho^{pp} = 0.131 \pm 0.0025$ at the LHC energy $\sqrt{s} = 14$TeV.

*ishida@phys.meisei-u.ac.jp

## I. INTRODUCTION

Recently there are several evidences[1, 2, 3, 4, 5, 6] of the total cross section $\sigma_{\rm tot}$ in the $\pi p$ and $\bar{p}(p)p$ scatterings to be proportional to $\log^2 s$ in high energies, consistent with the Froissart unitarity bound[7, 8]. The COMPETE collaborations[2, 6] have further assumed $\sigma_{\rm tot} \simeq B \log^2(s/s_0)$ to extend its universal rise with a common value of $B$ for all the hadronic scatterings. The universality of the coefficient $B$ was expected in the papers[9], and other theoretical supports[10, 11] based on the arguments describing deep inelastic scattering by gluon saturation in hadron light-cone wave function (the Colour Glass Condensate[12] of QCD) were given in recent years. There has been, however, no rigorous proof yet based on QCD.

Therefore, it is worthwhile to prove or disprove this universal rise of $\sigma_{\rm tot}$ even empirically. In the near future, the $pp$ total cross section $\sigma_{\rm tot}^{pp}$ in $\sqrt{s} = 14$TeV will be measured at TOTEM[13] and the other experiment[14] in the LHC. Therefore, the value of $B$ for $\bar{p}p, pp$ scattering, $B_{pp}$, will be determined with good accuracy. On the other hand, the $\pi^- N$ total cross sections $\sigma_{\rm tot}^{\pi^- N}$ have been measured only up to $k = 610$GeV where $k$ is the laboratory momentum of $\pi$ and it corresponds to $\sqrt{s} = 33.8$GeV, by the SELEX collaboration[15]. Thus, one might doubt to obtain the value of $B$ for $\pi p$ scattering, $B_{\pi p}$, with reasonable accuracy.

In the previous article[5], we attacked this problem by comparing the value of $B_{pp}$ and $B_{\pi p}$ in a new light. We used the laboratory energy of the incident particle, denoted as $\nu$, instead of the center of mass energy squared, $s$. They are related through

$$s \;=\; 2M\nu + M^2 + m^2 \tag{1}$$

with each other where $M$ is the mass of target proton and $m$ is the mass of incident particle: $m = \mu$(pion mass), $m = m_K$(kaon mass) and $m = M$ for $\pi p$, $Kp$ and $\bar{p}(p)p$ scatterings, respectively. The total cross section $\sigma_{\rm tot}$ is composed of crossing-even cross section $\sigma_{\rm tot}^{(+)}$ and crossing-odd cross section $\sigma_{\rm tot}^{(-)}$. Its definition will be given in Sec.2. The $\sigma_{\rm tot}^{(+)}$ is a sum of Reggeon component and non-Reggeon component and $\sigma_{\rm tot}^{(-)}$ is only made of Reggeon component corresponding to the vector meson trajectories. The Reggeon components become negligible in the high-energy region. Thus, the $\sigma_{\rm tot}$ in high energies is described only by the

non-Reggeon component of $\sigma_{\rm tot}^{(+)}$, which is parametrized by

$$\sigma_{\rm tot}^{(+)} \simeq \frac{4\pi}{m^2}\left(c_2 \log^2\frac{\nu}{m} + c_1 \log\frac{\nu}{m} + c_0\right) \quad . \tag{2}$$

The coefficients $c_2, c_1, c_0$ are introduced in the respective scatterings.

The equation (2) with $c_2 > 0$ shows the shape of parabola as a function of $\log\,\nu$ with a minimum. The $c_2$ parameter controls the rise of parabola in high-energy side. We re-express Eq. (2) as

$$\sigma_{\rm tot}^{(+)} \simeq Z^{ap} + B\,\log^2\frac{s}{s_0} \tag{3}$$

with $a = \pi^+, K^+, p$. By using the relation $s \simeq 2M\nu$ from Eq. (1) approximated in high energies, the $c_2$ in Eq. (2) is related directly with the $B$ parameter in Eq. (3). Thus, we obtain the $B$ parameters for the relevant processes individually. In the case of $\bar{p}p$, we have data for large values of $\log\,\nu$ coming from SPS and Tevatron experiments. Thus we can determine the value of $c_2(pp)$ and thus $B_{pp}$ with good accuracy. On the other hand, in the case of $\pi^- p, \pi^+ p$ scatterings we have used rich information of the experimental $\sigma_{\rm tot}$ data in the low and intermediate energy regions through the finite-energy sum rule (FESR). We used the FESR as a constraint between high-energy parameters, and analyzed the $\pi^\mp p$ total cross sections $\sigma_{\rm tot}^{\pi^\mp p}$ and the $\rho$ ratios $\rho^{\pi^\mp p}$, the ratios of real to imaginary parts of the forward scattering amplitudes. Here we adopted the FESR with the integral region between $k = \overline{N_1}$ and $\overline{N_2}$[16, 17]. The $k$ is the laboratory momentum of the incident particle which is related with $\nu$ by $k = \sqrt{\nu^2 - m^2}$. The $k \simeq \nu$ in high-energy regions. This FESR required that the low-energy extension of the high-energy asymptotic formula should coincide, roughly speaking, with the average of experimental $\sigma_{\rm tot}$ in the relevant region between $k = \overline{N_1}$ and $\overline{N_2}$. This requirement is called the FESR duality. We have already used [16, 17] this sum rule between $\overline{N_1} = 10$GeV and $\overline{N_2} = 20$GeV. The rich data in $k < 10$GeV were not included in this case, however. The lower-energy data are included in the integral of $\sigma_{\rm tot}$, the more precisely determined is the sub-leading term, i.e., the $P'$ term ( the term with coefficient $\beta_{P'}$ in Eq. (6) corresponding to $f_2(1275)$ trajectory), which is built in the sense of FESR[18, 19, 20] by the sum of direct channel resonances. Then, it helps to determine the non-leading term such as $\log\,\nu$ which then helps to determine the leading term like $\log^2\nu$. Thus, for the $\pi p$ scatterings, we are able to extend maximally the energy regions of the input data to take $\overline{N_1} \leq 10$GeV, so as to obtain the value of $B_{\pi p}$ as most accurately as possible.

It is to be noted that the $\bar{p}p$ scattering has open (meson) channels below $\bar{p}p$-threshold with $\nu < M$(corresponding to $\sqrt{s} < 2M$), and $\sigma_{\rm tot}^{(+)}$ diverges above the threshold($\nu > M$) because of the exothermic reactions. The $K^-p$ scattering has also open channels with $\nu < m_K$ (corresponding to $\sqrt{s} < M + m_K$). If we choose the value of $\overline{N_1}$ to be fairly larger than $m$ ($m = M$ for $\bar{p}p$, $m = m_K$ for $K^-p$), we have no difficulty coming from open channels. Contrarily, there are no such effects in $\pi p$ scattering . Thus, by taking $\overline{N_1}$ as small as possible, we can take into account more resonances through FESR in order to obtain the low-energy extension from the high-energy side with good accuracy. To obtain a sufficiently small error of $B_{\pi p}$, it appears to be important to include the information of the low-energy scattering data with $0 \leq k \leq 10$GeV through FESR.

We will show that the resulting value of $B_{\pi p}$ is consistent[5] with that of $B_{pp}$, which appears to support the universality hypothesis. It will also be shown that the central value of $B_{Kp}$ is also consistent with $B_{pp}$ and $B_{\pi p}$, although its error is fairly large, due to the present situation of the $K^-p$, $K^+p$ data. So far, we have searched for the simultaneous best fit of the high-energy parameters such as $c_2, c_1, c_0 \cdots$ to the $\sigma_{\rm tot}$ and the $\rho$ ratios under the duality constraint. In other words, both $B$(related to $c_2$) and $s_0$(related to $c_1/c_2$) was completely arbitrary.

We have also attempted to fit data by assuming the universality of $B$ in $\sigma_{\rm tot} \sim B \log^2(s/s_0)$ from the beginning. The fit is successful and the increase of total fitting $\chi^2$ due to the universality constraint is small. This result also suggests the universality of $B$. The scale $s_0$ has been assumed to be independent of the colliding particles in ref.[6]. This resulted in reducing the number of adjustable parameters. But there has been no proof again on this assumption based on QCD. We will also investigate this possibility.

In Sec.2, kinematical considerations are summarized for forward $\pi^{\mp}p$, $K^{\mp}p$ and $\bar{p}(p)p$ scatterings. A duality constraint is also explained based on the special form of FESR. In Sec. 3, we explain the approach how to estimate the value of $B$, $s_0$ and $Z$ individually for the above hadron scatterings. In Sec. 4, detailed analyses are given based on $\sigma_{\rm tot}$ and $\rho$ together with the duality constraint. We then discuss about the universality of coefficient $B$. Sec. 5 summarizes our conclusions.

## II. KINEMATICAL CONSIDERATIONS

### A. Total cross sections $\sigma_{\rm tot}$ and $\rho$ ratios

We take both the crossing-even and crossing-odd forward scattering amplitudes, $F^{(+)}(\nu)$ and $F^{(-)}(\nu)$, defined by

$$\begin{aligned} F^{(\pm)}(\nu) &= \frac{f^{\bar{a}p}(\nu) \pm f^{ap}(\nu)}{2} \\ f^{\bar{a}p}(\nu) &= F^{(+)}(\nu) + F^{(-)}(\nu) \\ f^{ap}(\nu) &= F^{(+)}(\nu) - F^{(-)}(\nu) \end{aligned} \tag{4}$$

where $(\bar{a}, a) = (\pi^-, \pi^+)$, $(K^-, K^+)$ and $(\bar{p}, p)$ respectively, and $f^{\bar{a}p}(\nu)$; $f^{ap}(\nu)$ is the forward $\bar{a}p$; $ap$ scattering amplitudes. The $\nu$ is the incident energy of $\bar{p}(p)$, $\pi$ and $K$ in the laboratory system. The combinations (4) of the amplitudes satisfy the crossing property

$$F^{(\pm)}(-\nu) = \pm F^{(\pm)}(\nu)^* \tag{5}$$

under crossing transformation $\nu \to -\nu$ for forward amplitudes. We assume that

$$\mathrm{Im}F^{(+)}(\nu) \simeq \frac{\nu}{m^2}\left(c_0 + c_1 \log\frac{\nu}{m} + c_2 \log^2\frac{\nu}{m}\right) + \frac{\beta_{P'}}{m}\left(\frac{\nu}{m}\right)^{\alpha_{P'}} \tag{6}$$

$$\mathrm{Im}F^{(-)}(\nu) \simeq \frac{\beta_V}{m}\left(\frac{\nu}{m}\right)^{\alpha_V} , \tag{7}$$

for $\nu > N$ with some energy $N$ due to the Pomeron-Reggeon exchange model except for the terms with coefficients $c_2$ and $c_1$ . The coupling coefficients $\beta_{P'},\ c_0,\ \beta_V$ are the unknown parameters in the Regge theory. The $\alpha_{P'},\ \alpha_V$ are determined phenomenologically. The $c_2,\ c_1$ terms are introduced consistently with the Froissart bound to describe the rise of $\sigma_{\rm tot}$ in the high-energy regions. The total cross sections $\sigma_{\rm tot}^{\bar{a}p},\ \sigma_{\rm tot}^{ap}$ and the $\rho$ ratios $\rho^{\bar{a}p}$ and $\rho^{ap}$ are given by

$$\begin{aligned} \mathrm{Im}\ f^{\bar{a}p,ap}(\nu) &= \frac{k}{4\pi}\sigma_{\rm tot}^{\bar{a}p,ap} , \\ \rho^{\bar{a}p} &= \frac{\mathrm{Re}\ f^{\bar{a}p}}{\mathrm{Im}\ f^{\bar{a}p}}, \quad \rho^{ap} = \frac{\mathrm{Re}\ f^{ap}}{\mathrm{Im}\ f^{ap}}, \end{aligned} \tag{8}$$

respectively, where the $k$ are the incident momenta of $\bar{p}(p),\ \pi$ and $K$ in the laboratory system. The total cross section of crossing-even(odd) part $\sigma_{\rm tot}^{(\pm)}$ is given by $\sigma_{\rm tot}^{(\pm)} = (\sigma_{\rm tot}^{\bar{a}p} \pm \sigma_{\rm tot}^{ap})/2 = \frac{4\pi}{k}\mathrm{Im}F^{(\pm)}(\nu)$. By using the crossing property (5), the real parts are given by[4, 17]

$$\mathrm{Re}F^{(+)}(\nu) \simeq \frac{\pi\nu}{2m^2}\left(c_1 + 2c_2 \ln\frac{\nu}{m}\right) - \frac{\beta_{P'}}{m}\left(\frac{\nu}{m}\right)^{\alpha_{P'}} \cot\frac{\pi\alpha_{P'}}{2} + F^{(+)}(0) , \tag{9}$$

$$\mathrm{Re}F^{(-)}(\nu) \simeq \frac{\beta_V}{m}\left(\frac{\nu}{m}\right)^{\alpha_V} \tan\frac{\pi\alpha_V}{2} , \tag{10}$$

where $F^{(+)}(0)$ is a subtraction constant.

### B. Duality constraints

The FESR is used as a duality constraint between these parameters[16, 17].

$$\frac{2}{\pi}\int_{N_1}^{N_2} \quad \frac{\nu}{k^2}\,\mathrm{Im}F^{(+)}(\nu)\;d\nu = \frac{1}{2\pi^2}\int_{\overline{N}_1}^{\overline{N}_2}\;\sigma_{\rm tot}^{(+)}(k)\;dk \quad . \tag{11}$$

The laboratory energy $\nu$ is related with corresponding momentum $k$ by $\nu=\sqrt{k^2+m^2}$. The momentum corresponding to $\nu = N$ is represented by the quantity with overline such as $k=\overline{N}$ in this paper. The $\nu = N_{1,2}$ in Eq. (11) are related to the corresponding momenta $k=\overline{N_{1,2}}$ by $N_{1,2}=\sqrt{\overline{N_{1,2}}^2+m^2}$. The value of $\overline{N_2}$ should be selected to be reasonably high momentum above which no resonance structures are observed, while $\overline{N_1}$ may be taken to be in the resonance region in the sense of the FESR duality.

The integrand of the LHS of Eq. (11) is the low-energy extension of Eq. (6). The RHS is the integral of experimental $\sigma_{\rm tot}^{(+)}(=(\sigma_{\rm tot}^{\bar{a}p}+\sigma_{\rm tot}^{ap})/2)$ in the resonance-energy regions. This shows up several peak and dip structures corresponding to a number of resonances, in addition to the non-resonating background. Thus, Eq. (11) means the FESR duality, that is, the average of these resonance structures plus the non-resonating background in $\sigma_{\rm tot}^{(+)}$ should coincide with the low-energy extension of the asymptotic formula.

## III. THE GENERAL APPROACH

### A. Energy region of $\sigma_{\rm tot}$ and $\rho$ fitted by asymptotic formulas

Let us first discuss the energy regions where experimental $\sigma_{\rm tot}$ and $\rho$ ratios can be fitted by the asymptotic forms (6)-(10).

As is well known, many low-energy resonances smoothly join into the smooth high-energy behviours around the transition energy $\nu_0$. This energy $\nu_0$ are around 5GeV (which corresponds to $\sqrt{s}\simeq 3.3$GeV in $\bar{p}p$ scattering) in real experimental data. This value of $\nu_0$ are in the energy region of overlapping resonances and seems to be too small to apply the asymptotic formula to the data just above $\nu=\nu_0$. However, since the average of low-energy resonances is equivalent to the asymptotic formula due to the FESR duality, we can equate

the experimental $\sigma_{\rm tot}$ to the imaginary part of $F^{(\pm)}(\nu)$ (6),(7) for $\nu > \nu_0$. Let us now consider the behaviours of the real part of the amplitude. As a simplicity of explanation, let us consider the crossing-odd amplitude. Then, we can substitute the RHS of (7) into the principal part dispersion integral, instead of substituting low-energy resonances, due to the FESR duality. Therefore, we can obtain the RHS of (10) explicitly for $\nu > \nu_0$.

This can be easily extended to the general case. When the scattering amplitude includes the contribution from the Pomeron exchange, the two-component hypothesis of duality was proposed by Gilman,Harari and Zarmi[21], i.e., the ordinary Regge pole ( $P'$ ) are built by direct-channel resonances in the sense of FESR, while the Pomeron-type singularity (which corresponds to Eq. (2) in the present case) is associated with the non-resonating background. If we take this hypothesis, the same argument can be applied, and we can substitute the RHS of (6) into the principal-part dispersion relation from threshold to obtain the RHS of (9). Therefore, we can use the RHS of (9) for $\nu > \nu_0$. Since the transition energy $\nu_0$ is around 5GeV as mentioned above, we can use the asymptotic form for both the imaginary part and real part for $k > 5$GeV.

### B. Practical approach for the search of $B$

In order to obtain the value of $B$, we search for the simultaneous best fit to $\sigma_{\rm tot}^{(+)}$ and the $\rho^{(+)}$ ratios under the duality constraint, Eq.(11). The formula (4)—(10) and the duality constraint (11) are our starting points. The LHS of Eq. (11) is the integral of the asymptotic formulas (6) and is represented by a linear homogeneous equation of the parameters $c_{2,1,0}$ and $\beta_{P'}$. The RHS of Eq. (11) is the integral of experimental $\sigma_{\rm tot}$, which is estimated by using the experimental data of $\sigma_{\rm tot}^{\pi^{\mp}p}, \sigma_{\rm tot}^{K^{\mp}p}, \sigma_{\rm tot}^{\bar{p}p,pp}$. Here $\overline{N_2}$ is fixed to be 20GeV while we take various values of $\overline{N_1}$ being less than 10GeV. We try to take $\overline{N_1}$ as small as possible. The $\sigma_{\rm tot}^{\bar{a}p,ap}$ and $\rho^{\bar{a}p,ap}$ are fitted simultaneously for the respective processes of $\pi p$, $Kp$ and $\bar{p}(p)p$ scatterings. In actual analyses we fit the data of Re $f^{\bar{a}p,ap}(k)$ by the formulas (9) and (10). We have made them from experimental data of $\rho^{\bar{a}p,ap}$ in ref.[6] times Im $f_{\rm PDG}^{\bar{a}p,ap}(k)$ where we use the result of the fit given in PDG[6][40]. By using Re $f^{\bar{a}p,ap}$ data in the fittings, the resulting $\chi^2$ functions become second-order homogeneous equations of the relevant parameters, which are easy handle. It makes our analyses simple and transparent.

The $\sigma_{\rm tot}^{\bar{a}p,ap}$ for $k \geq 20$GeV and $\rho^{\bar{a}p,ap}$ for $k \geq 5$GeV are fitted simultaneously. Here, by

considering the transition energy $\nu_0 \sim 5$GeV, we have chosen $k \geq 5$GeV for the fitted energy region of the $\rho$ data, while for $\sigma_{\rm tot}$, $k \geq 20$GeV, being different from the $\rho$ data. The $\sigma_{\rm tot}$ data up to $k = 20$GeV are used to obtain their integrals in the duality constraint (11). Thus, in order to avoid the double-counting of the data we use larger values $k > 20$GeV for $\sigma$ than that for $\rho$.

The high-energy parameters $c_2, c_1, c_0, \beta_{P'}$ and $\beta_V$ are treated as process-dependent, while $\alpha_{P'}$ and $\alpha_V$ are fixed with common values for every process. The duality constraints (11) give constraints between $c_2, c_1, c_0$ and $\beta_{P'}$ for $\bar{p}(p)p$, $Kp$ and $\pi p$ scatterings, respectively. The $F^{(+)}(0)$ is treated as an additional parameter, and the number of fitting parameters is five for each process. The resulting $c_2$ are related to the $B$ parameters, defined by $\sigma \simeq B\log^2(s/s_0) + \cdots$, through the equation

$$B_{ap} \;=\; \frac{4\pi}{m^2} c_2, \quad m = M, \mu, m_K, \quad a = p, \pi, K \tag{12}$$

and we can test the universality of the $B$ parameters.

### C. Analysis when coefficient $B$, scale $s_0$ are assumed to be universal

We also analyze the data by assuming the coefficient $B$ of $\sigma_{\rm tot} \sim B\ \log^2(s/s_0)$ to be universal from the beginning and test the universality of $B$. We also search for the possibility that the $s_0$ has a common value for $pp$, $\pi p$, $Kp$ scatterings.

## IV. ANALYSIS BASED ON $\sigma_{\rm tot}$ AND $\rho$

### A. Evaluation of the integral of $\sigma_{\rm tot}^{(+)}$ appearing in FESR

In order to obtain the explicit forms of FESR (11), it is necessary to evaluate the integral of $\sigma_{\rm tot}^{(+)}$,

$$\frac{1}{2\pi^2}\int_{N_1}^{N_2} \sigma_{\rm tot}^{(+)}(k)\ dk \;=\; \frac{1}{2\pi^2}\int_{N_1}^{N_2} \frac{1}{2}(\sigma_{\rm tot}^{\bar{a}p}(k) + \sigma_{\rm tot}^{ap}(k))\ dk \tag{13}$$

with $a = \pi^+, K^+, p$ from the experimental data[6] for each process. For this purpose we have performed phenomenological fits to the experimental $\sigma_{\rm tot}^{\bar{a}p,ap}$. The experimental $\sigma_{\rm tot}$ can be fitted simply by the phenomenological formula $\sigma_{\rm tot} = \frac{4\pi}{k}\{\frac{\nu}{m^2}(c_2\log^2\frac{\nu}{m} + c_1\log\frac{\nu}{m} + c_0) +$

$\frac{\beta}{m}(\frac{\nu}{m})^{0.5} + \frac{d}{m}(\frac{\nu}{m})^{-0.5} + \frac{f}{m}(\frac{\nu}{m})^{-1.5} + \frac{g}{m}(\frac{\nu}{m})^{-2.5}\}$. The dimensionless parameters $c_2$ are fixed to the values of our previous analysis[16], $c_2 = 0.00140,\ 0.0185$ and $0.0520$ for $\pi^{\mp}p,\ K^{\mp}p$ and $\bar{p}(p)p$ scatterings, respectively. The other parameters are taken to be free, dependent on the processes. The error of each data point, denoted as $\Delta y$, is given by combining statistical error $\Delta y_{\rm stat}$ and systematic error $\Delta y_{syst}$ as $\Delta y \equiv \sqrt{(\Delta y_{\rm stat})^2 + (\Delta y_{\rm syst})^2}$. The data of $\sigma_{\rm tot}^{\bar{p}p}$ are mutually inconsistent in the low-energy region among the data of different experiments, and we cannot obtain a good fit. We adopt a statistical method, Sieve algorithm[22], and seven points are removed following this prescription[41]. The experimental $\sigma_{\rm tot}^{\bar{a}p,ap}(k)$ are fitted in the region of laboratory momenta, $k_a < k < 100$GeV, where $k_a$ are taken to be 3GeV, 2GeV and 2.5GeV for $\pi p, Kp$ and $\bar{p}(p)p$ scatterings, respectively. The $k_a$ correspond to $\sqrt{s} = 2.56$GeV, 2.35GeV and 2.60GeV for the relevant processes. There are no remarkable resonance structures observed above these energies, and successful fits are obtained by using commonly this simple formula. The $g$ is fixed to be $g = 0$ for the analyses of $\pi^{\mp}p$ and $\bar{p}(p)p$, while it is treated to be free for $K^{\mp}p$. The number of fitting parameters are 5 respectively for $\pi^{-}p$, $\pi^{+}p$, $\bar{p}p$ and $pp$, while 6 for $K^{-}p$ and for $K^{+}p$. The resulting $\chi^2$ are $\chi^2/(N_D - N_P) = 102.6/(165-5), 69.7/(100-5)$ for $\pi^{-}p, \pi^{+}p$; $171.4/(149-6), 75.0/(86-6)$ for $K^{-}p, K^{+}p$; $48.8/(70-5), 112.2/(103-5)$ for $\bar{p}p, pp$[42].

In the FESR (11) the $\overline{N_2}$ is fixed to be $\overline{N_2} = 20$GeV, while we take various values of $\overline{N_1}$. The integrals of $\sigma_{\rm tot}^{(+)}(k)$ from the relevant $\overline{N_1}$ to the $\overline{N_2}$ are estimated by using these phenomenological fits.

In $\pi p$ scatterings, we try to take very small values of $\overline{N_1}$ in the resonance-energy region. There are no open channels below threshold $\nu < \mu$ in this process, and the smaller value of $\overline{N_1}$ is taken, the more information in the low-energy region is included through FESR, and the more accurate value of $c_2$ is obtained. Actually we take $\overline{N_1}$ less than 1GeV. In this case we divide the region of the integral into two parts: The integral of $\sigma_{\rm tot}^{(+)}(k)$ from the higher-energy region, $k_d < k < \overline{N_2}$, is estimated by using the phenomenological fits, while the integral from the lower-energy region, $\overline{N_1} < k < k_d$, are evaluated directly from experimental data. That is, the data points are connected by straight lines and the areas of these polygonal line graphs are regarded as the corresponding integrals. The dividing momentum $k_d$ is taken to be 4GeV.

The $\sigma_{\rm tot}^{\pi^{\mp}p}$ data in low-energy region are shown in Fig. 1.

We take $k$=$\overline{N_1}$=10,7,5,4,3.02,2.035,1.476,0.9958,0.818,0.723,0.475,0.281 GeV. These values

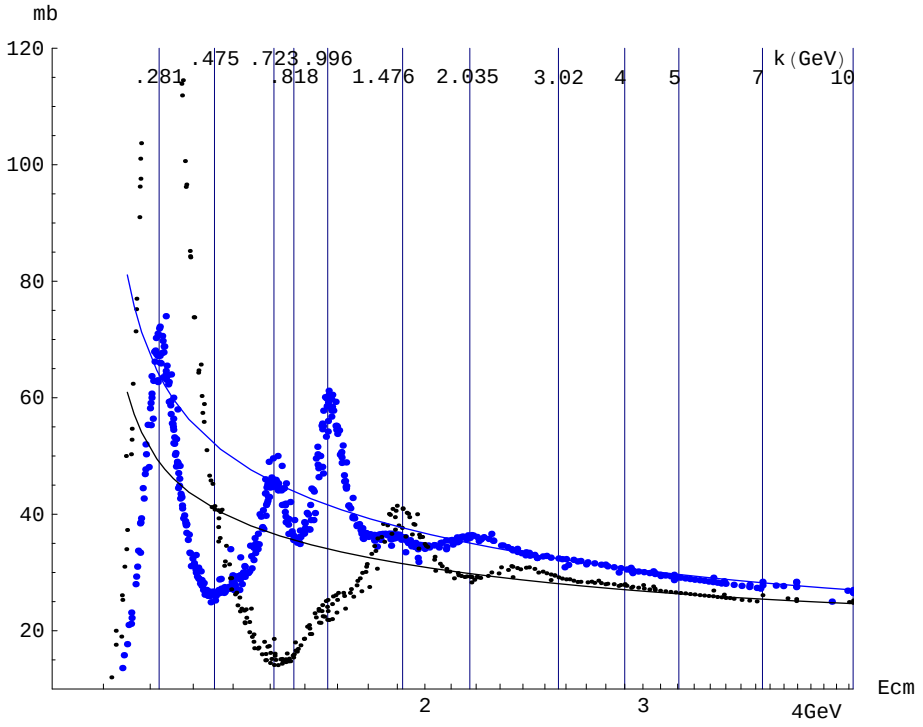


FIG. 1: The $\sigma_{\rm tot}$ data of $\pi^- p$ scattering(big blue points) and of $\pi^+ p$ scattering(small black points) in the low-energy region: The errors are not shown. The horizontal axis represents center of mass energy $E_{cm}$. The vertical lines correspond to the values of laboratory momenta $k$=$\overline{N_1}$=10,7,5,4,3.02,2.035,1.476,0.9958,0.818,0.723,0.475,0.281 GeV, which are selected as the lower limits of the integrals in FESR (11). Their numbers(in GeV) are shown in the upper side. The solid lines represent the low-energy extensions of our best fit using FESR in the case $\overline{N_1} = 0.818$GeV.

of $\overline{N_1}$, which are shown by vertical lines, correspond to the laboratory momenta of peak and dip positions observed in experimental $\sigma_{\rm tot}^{\pi^\mp p}$ spectra. This can be seen in Fig. 1.

The values of cross-section integrals estimated from the above-mentioned procedures are given in Table I.

Situations are different in $K^\mp p$ and $\bar{p}p, pp$ scatterings. The $K^- p$ is the exothermic reaction. $K^- p \to \pi^0\Lambda, \pi\Sigma$ could occur even at threshold $\nu = m_K$, and the $\sigma_{\rm tot}^{K^- p}(k)$ increases like $1/k$ near threshold. In the case of too small values of $\overline{N_1}$, the integral of $\sigma_{\rm tot}$ is affected strongly by the contribution from these open channels. Furthermore, in the exotic $K^+ p$ channel there is a sudden decrease of $\sigma_{\rm tot}$ observed below $E_{cm} \simeq 1.9$GeV($k \simeq 1.2$GeV). Similarly, $\bar{p}p$ has a number of open meson channels below threshold, $\nu < M$, and a big dip

TABLE I: The integral of cross section $\frac{1}{2\pi^2}\int_{\overline{N_1}}^{\overline{N_2}}\sigma_{\rm tot}^{\pi^{\mp}p}(k)\,dk$ ($\mathrm{GeV}^{-1}$) and their average estimated by using experimental data for $\pi^{\mp}p$ scattering: The $\overline{N_2}$ is fixed to be 20GeV while we take various values of $\overline{N_1}$.

| $\overline{N_1}$–$\overline{N_2}$(GeV) | $\frac{1}{2\pi^2}\int_{\overline{N_1}}^{\overline{N_2}}\sigma_{\rm tot}^{\pi^-p}(k)\,dk$ | $\frac{1}{2\pi^2}\int_{\overline{N_1}}^{\overline{N_2}}\sigma_{\rm tot}^{\pi^+p}(k)\,dk$ | $\frac{1}{2\pi^2}\int_{\overline{N_1}}^{\overline{N_2}}\sigma_{\rm tot}^{(+)}(k)\,dk$ |
|---|---|---|---|
| 10–20 | 31.404±0.033 | 33.611±0.029 | 32.508±0.022 |
| 7–20 | 41.253±0.042 | 44.244±0.038 | 42.748±0.028 |
| 5–20 | 48.069±0.047 | 51.656±0.044 | 49.863±0.032 |
| 4–20 | 51.609±0.048 | 55.536±0.047 | 53.572±0.034 |
| 3.02–20 | 55.220±0.050 | 59.539±0.052 | 57.380±0.036 |
| 2.035-20 | 59.069±0.052 | 63.899±0.053 | 61.484±0.037 |
| 1.476–20 | 61.456±0.052 | 66.443±0.054 | 63.950±0.038 |
| 0.9958-20 | 63.431±0.053 | 68.994±0.056 | 66.213±0.039 |
| 0.818–20 | 63.907±0.053 | 70.016±0.057 | 66.961±0.039 |
| 0.723–20 | 64.093±0.053 | 70.536±0.057 | 67.314±0.039 |
| 0.475–20 | 64.875±0.053 | 71.605±0.057 | 68.240±0.039 |
| 0.281–20 | 67.563±0.054 | 72.646±0.057 | 70.105±0.039 |

structure is observed in $\sigma_{\rm tot}$ of exotic $pp$ channel below $E_{cm}\simeq 2.2\mathrm{GeV}(k\simeq 1.4\mathrm{GeV})$. We can see the situations in the $\sigma_{\rm tot}^{K^{\mp}p}$ and $\sigma_{\rm tot}^{\bar{p}p,pp}$ data shown in Figs. 2 and 3, respectively. The reason for producing these strucures is not known, but it is safe to take $\overline{N_1}$ to be fairly larger than $m_K$ and $M$. Actually we take $\overline{N_1}\geq 3\mathrm{GeV}$ as $\overline{N_1}=10,7,5,4,3\mathrm{GeV}$ in $K^{\mp}p$ and $\bar{p}p,pp$ scatterings. These laboratory momenta are represented by vertical lines in Fig.2 and 3, respectively.

For each value of $\overline{N_1}$ the integrals of $\sigma_{\rm tot}^{\bar{a}p,ap}$ and their average $\sigma_{\rm tot}^{(+)}$ are estimated by using the phenomenological fits to $K^{\mp}p$ and $\bar{p}(p)p$ scatterings. The results are given in Tables II and III, respectively.

The values of integrals given in Tables I, II and III are estimated with very small errors, which are generally less than 0.3% . We regard central values as exact ones and treat the FESR (11) as exact constraints between the fitting parameters.

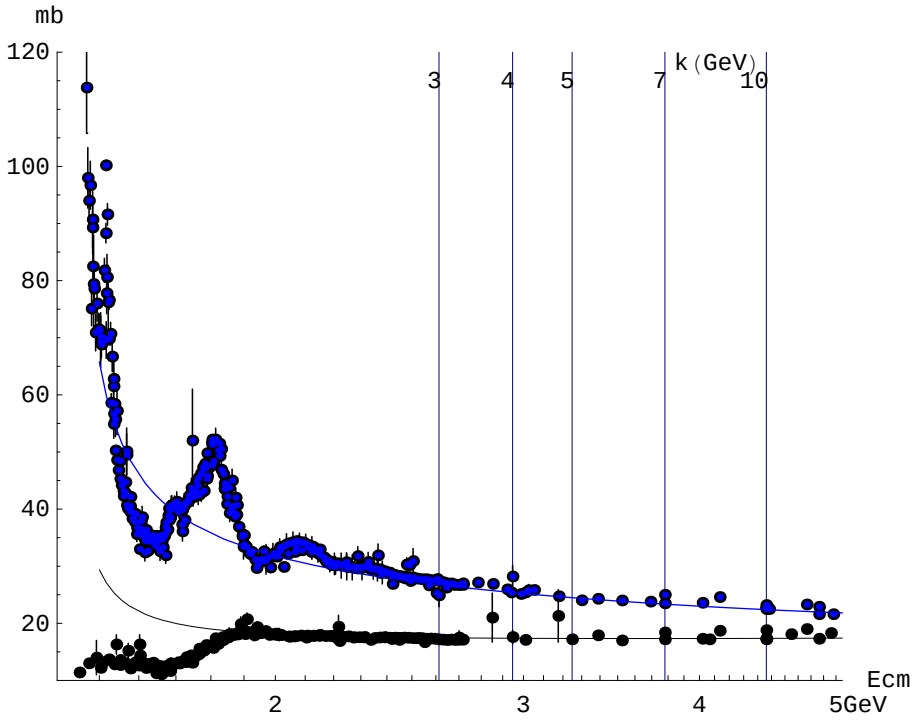


FIG. 2: The experimental $\sigma_{\rm tot}$ of $K^-p$(blue points) and of $K^+p$(black points) in the low-energy region: The vertical lines correspond to the laboratory momenta $k$=$\overline{N_1}$=10,7,5,4,3 GeV, which are selected as the lower limits of the FESR integrals (11). Their numbers(in GeV) are shown in the upper side. The horizontal axis represents corrresponding center of mass energy $E_{cm}$. The solid lines represent the low-energy extensions of our best fit using FESR in the case $\overline{N_1} = 5$GeV.

### B. Analysis of $\pi^{\mp}p$ scattering

The data[6] of $\sigma_{\rm tot}^{\pi^{\mp}p}$ for $k \geq 20$ GeV and $\rho^{\pi^{\mp}p}$ (more exactly Re $f^{\pi^{\mp}p}$) for $k \geq 5$ GeV are fitted simultaneously. In the FESR (11), $\overline{N_2}$ is taken to be 20GeV. The $\overline{N_1}$ are chosen to be 10, 7, 5, 4, 3.02, 2.035, 1.476, 0.9958, 0.818, 0.723, 0.475, 0.281 GeV, as explained before.

For each value of $\overline{N_1}$, the integrals of $\sigma_{\rm tot}^{(+)}$ which are the RHS of Eq. (11) are given in Table I. The integral of asymptotic formula (6) which appears in the LHS of Eq. (11) is calculable analytically, and we obtain the explicit form of FESR (11). In the case of $\overline{N_1} = 0.818$GeV, for example, the FESR (11) is given by

$$(\pi p) \qquad 87.1714\beta_{P'} + 627.26c_0 + 2572.37c_1 + 10891.2c_2 = 66.961 \pm 0.039\ . \tag{14}$$

The error of the RHS is very small, and Eq. (14) is regarded as an exact constraint between the parameters, $c_{2,1,0}$ and $\beta_{P'}$. The $\beta_{P'}$ is represented by the other three parameters $c_{2,1,0}$

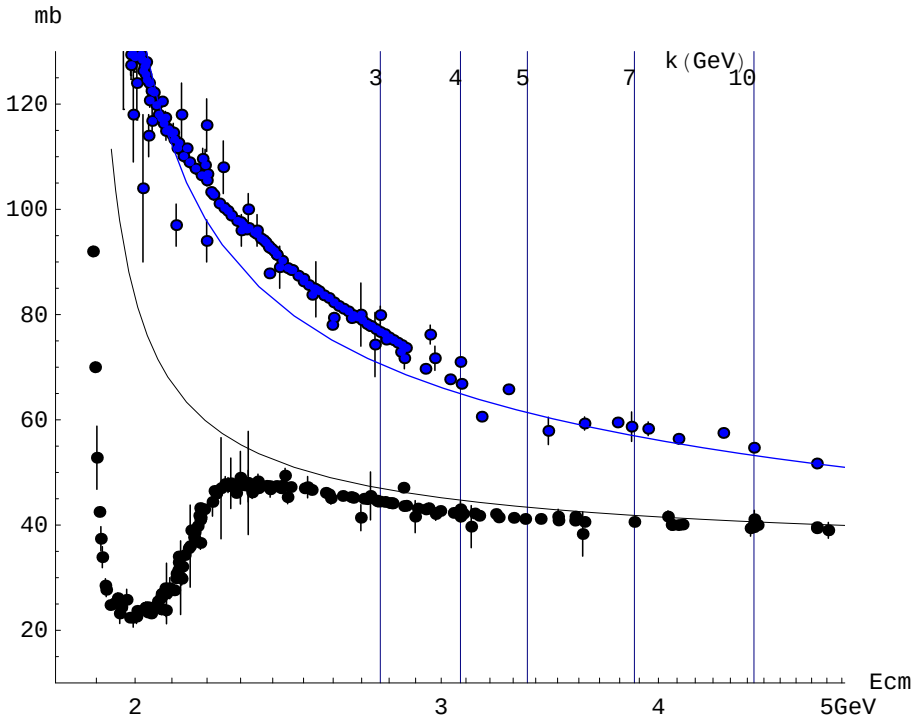


FIG. 3: The experimental $\sigma_{\rm tot}$ of $\bar{p}p$(blue points) and of $pp$(black points) in low-energy region: The vertical lines correspond to the values of $k = \overline{N_1}$ selected in our analyses. See, the caption in Fig.2.

TABLE II: The integral of $\sigma_{\rm tot}$ in $K^{\mp}p$: $\frac{1}{2\pi^2}\int_{\overline{N_1}}^{\overline{N_2}} \sigma_{\rm tot}^{K^-p,K^+p,(+)}(k)\ dk$ (GeV$^{-1}$). The $\overline{N_2}$ is taken to be 20GeV while $\overline{N_1}$ are taken to be 10,7,5,4,3GeV, respectively.

| $\overline{N_1}$–$\overline{N_2}$(GeV) | $\frac{1}{2\pi^2}\int_{\overline{N_1}}^{\overline{N_2}} \sigma_{\rm tot}^{K^-p}(k)\ dk$ | $\frac{1}{2\pi^2}\int_{\overline{N_1}}^{\overline{N_2}} \sigma_{\rm tot}^{K^+p}(k)\ dk$ | $\frac{1}{2\pi^2}\int_{\overline{N_1}}^{\overline{N_2}} \sigma_{\rm tot}^{(+)}(k)\ dk$ |
|---|---|---|---|
| 10–20 | 28.217±0.068 | 22.661±0.053 | 25.439±0.043 |
| 7–20 | 37.175±0.094 | 29.377±0.069 | 33.276±0.058 |
| 5–20 | 43.425±0.110 | 33.818±0.077 | 38.622±0.067 |
| 4–20 | 46.693±0.116 | 36.031±0.080 | 41.362±0.070 |
| 3–20 | 50.120±0.120 | 38.257±0.081 | 44.189±0.072 |

as $\beta_{P'} = \beta_{P'}(c_2, c_1, c_0)$. The fitting is performed with five parameters, including $\beta_V$ and $F^{(+)}(0)$. The $(\alpha_{P'}, \alpha_V)$ in Eqs. (6) and (7) are fixed to be empirical values $(0.500, 0.497)$[16] in all the fitting procedures. The values of $c_2$ and $\chi^2$ in the best fits for the respective $\overline{N_1}$ are given in Tables IV[43].

As is seen in Table IV, values of the best fitted $c_2$ are almost independent of the choices of $\overline{N_1}$ (except for the case $\overline{N_1}$=0.475GeV). The results are surprisingly stable, although there

TABLE III: The integral of $\sigma_{\rm tot}$ in $\bar{p}p, pp$: $\frac{1}{2\pi^2}\int_{\overline{N_1}}^{\overline{N_2}} \sigma_{\rm tot}^{\bar{p}p,pp,(+)}(k)\ dk$ (GeV$^{-1}$). The $\overline{N_2}$ is taken to be 20GeV, while $\overline{N_1}$ is taken to be 10,7,5,4,3GeV.

| $\overline{N_1}$–$\overline{N_2}$(GeV) | $\frac{1}{2\pi^2}\int_{\overline{N_1}}^{\overline{N_2}} \sigma_{\rm tot}^{\bar{p}p}(k)\ dk$ | $\frac{1}{2\pi^2}\int_{\overline{N_1}}^{\overline{N_2}} \sigma_{\rm tot}^{pp}(k)\ dk$ | $\frac{1}{2\pi^2}\int_{\overline{N_1}}^{\overline{N_2}} \sigma_{\rm tot}^{(+)}(k)\ dk$ |
|---|---|---|---|
| 10–20 | 65.75±0.24 | 51.07±0.06 | 58.41±0.12 |
| 7–20 | 87.61±0.33 | 66.68±0.07 | 77.14±0.17 |
| 5–20 | 103.48±0.39 | 77.28±0.08 | 90.38±0.20 |
| 4–20 | 112.11±0.41 | 82.72±0.08 | 97.41±0.21 |
| 3–20 | 121.51±0.41 | 88.33±0.08 | 104.92±0.21 |

TABLE IV: Values of $c_2$ of $\pi p$ scattering in the best fit with five-parameters, using FESR as a constraint. The fitting $\chi^2$ are given in the next row. The number of data points is 162. The result of six-parameter fit without using FESR is also shown in the last column as No SR.

| $\overline{N_1}$ | 10 | 7 | 5 | 4 | 3.02 | 2.035 | 1.476 |
|---|---|---|---|---|---|---|---|
| $c_2(10^{-5})$ | 142(21) | 136(19) | 132(18) | 129(17) | 124(16) | 117(15) | 116(14) |
| $\chi^2_{\rm tot}$ | 149.05 | 149.35 | 149.65 | 149.93 | 150.44 | 151.25 | 151.38 |
| $\overline{N_1}$ | 0.9958 | 0.818 | 0.723 | 0.475 | 0.281 | | No SR |
| $c_2(10^{-5})$ | 116(14) | 121(13) | 126(13) | 140(13) | 121(12) | | 164(29) |
| $\chi^2_{\rm tot}$ | 151.30 | 150.51 | 149.90 | 148.61 | 150.39 | | 147.78 |

are many resonant strucures and $\sigma_{\rm tot}^{\pi^\mp p}$ show sharp peak and dip structures in this energy region.

We can adopt the case of $\overline{N_1}$=0.818GeV as a representative of our results. The best-fit value of $c_2$ is

$$c_2 \ = \ (121 \pm 13) \cdot 10^{-5} \quad . \tag{15}$$

The best-fit values of the other parameters are given in Table V.

The result should be compared to the analysis with no use of FESR. In this case there is no constraint between parameters, and the fitting is performed with six parameters including $\beta_{P'}$. The value of $c_2$ in the best fit is

$$c_2 \ = \ (164 \pm 29) \cdot 10^{-5} \quad . \tag{16}$$

TABLE V: Values of best-fitted parameters and their one-standard deviations in $\pi^{\mp}p$ scattering. The FESR with $\overline{N_1}$=0.818GeV is used and $\beta_{P'}$ is obtained from the other parameters by using this FESR. Our predicted lines in Fig. 5 are depicted by using these values.

| $c_2(10^{-5})$ | $c_1$ | $c_0$ | $F^{(+)}(0)$ | $\beta_V$ | $\beta_{P'}$ |
|---|---|---|---|---|---|
| 121.1 | -0.01179 | 0.1141 | -0.0180 | 0.04004 | 0.1437 |
| +13.3 | -0.01385 | 0.1224 | -0.2785 | 0.03991 | 0.1280 |
| −13.3 | -0.00974 | 0.1058 | 0.2425 | 0.04018 | 0.1594 |

This value should be compared with the result (15) using FESR. By including rich information of low-energy scattering data in the form of FESR, the error of $c_2$ in Eq. (15) becomes less than half of Eq. (16).

Predicted spectra of $\sigma_{\rm tot}$ with no use of FESR are shown in Fig. 4 and with using FESR in Fig. 5. The uncertainties of the prediction by the best fit are shown by shaded region in Figs. 4 and 5, which corresponds to $c_2$ in Eqs. (16) and (15), respectively. Our prediction in Fig.5 is greatly improved from that in Fig. 4.

The result of the fit to $\rho^{\pi^{\mp}p}$ are given in Fig. 6.

The $c_2\log^2\frac{\nu}{\mu}+c_1\log\frac{\nu}{\mu}$ with $c_2>0$ shows the shape of parabola as a function of $\log\frac{\nu}{\mu}$ with minimum. In order to determine the $c_2, c_1$ coefficients of $\log^2\frac{\nu}{\mu}$ and $\log\frac{\nu}{\mu}$ with a sufficient accuracy, a few orders of magnitude are neccesary for fitted energy region. The fitted energy region for $\pi^-p$ is 20GeV$< k <$ 370GeV for $\pi^-p$ shown by horizontal arrow in the figure, which corresponds to 6.2GeV$< E_{cm}(\equiv\sqrt{s})<$26.4GeV. This energy range is insufficient to determine $c_2$ with enough accuracy.

The energy region of the FESR integral, $\overline{N_1}$(=0.818GeV)$< k <$20GeV (which corresponds to $1.56<\sqrt{s}=E_{cm}<6.2$GeV), is shown by double horizontal arrow in Fig. 5. Additional information from this energy region greatly helps to improve our estimate of $c_2$. It is very important to include the information of the data in low-energy region by using FESR.

The value of $\sigma_{\rm tot}$ in $\pi^-N$ scattering at $k=610$GeV($E_{cm}=33.8$GeV) is reported by SELEX collaboration[15] as $\sigma_{\rm tot}^{\pi N}=26.6\pm0.9$mb. Here $N$ is not identified with proton or neutron. Our prediction of $\sigma_{\rm tot}^{(+)}(=(\sigma_{\rm tot}^{\pi^-p}+\sigma_{\rm tot}^{\pi^+p})/2)$ at this energy is $25.75\pm0.05$mb, and $\sigma_{\rm tot}^{\pi^-p}-\sigma_{\rm tot}^{\pi^+p}$ is 0.30mb. By taking this value into account we may predict $\sigma_{\rm tot}^{\pi^-N}=25.8\pm0.3$mb at $k$=610GeV. It is consistent with the SELEX measurement.

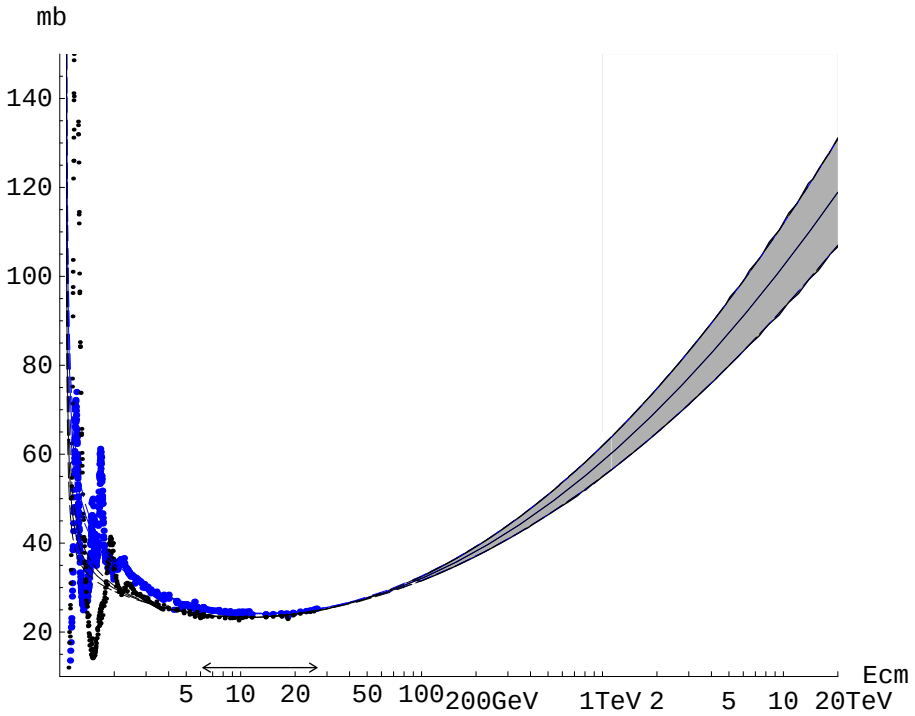


FIG. 4: Prediction of $\sigma_{\rm tot}^{\pi p}$ with No use of FESR The data points are given with no error bars. The big blue points (line) are data (best-fitted curve) for $\pi^- p$. The black points and lines are for $\pi^+ p$. The horizontal arrow represents the energy region of the fitting. The shaded region corresponds to the uncertainty of the prediction by the best fit, where $c_2 = (164 \pm 29) \times 10^{-5}$. The $c_2$ has large uncertainty since it is not determined well by direct fitting of the data above $k = 20\text{GeV}(E_{cm} = 6.2\text{GeV})$.

In Fig. 1, our best fitted curve in the case of $\overline{N_1} = 0.818\text{GeV}$ is also depicted. The fitted energy region is above $k = 20\text{GeV}(E_{cm} = 6.2\text{GeV})$, and it is far above the energy region shown in this Fig.1. Nevertheless, the low-energy extensions of the asymptotic formula almost coincide with the experimental $\sigma_{\rm tot}^{\pi^\mp p}$ in $E_{cm}$ up to $\sim 3\text{GeV}$, and in $E_{cm} <\sim 3\text{GeV}$ they seem to cross the averages of peak and dip structures of various $N$ and $\Delta$ resonances. This shows that the FESR duality is satisfied in our best fit.

### C. Analysis of $K^\mp p$ scattering

The $K^- p$ and $K^+ p$ scatterings are analyzed by the same method. We fix $\overline{N_2} = 20\text{GeV}$ while we take various values of $\overline{N_1}$ as $\overline{N_1} = 10, 7, 5, 4, 3\text{GeV}$. The integral of $\sigma_{\rm tot}^{(+)}$ $(= (\sigma_{\rm tot}^{K^- p} +$

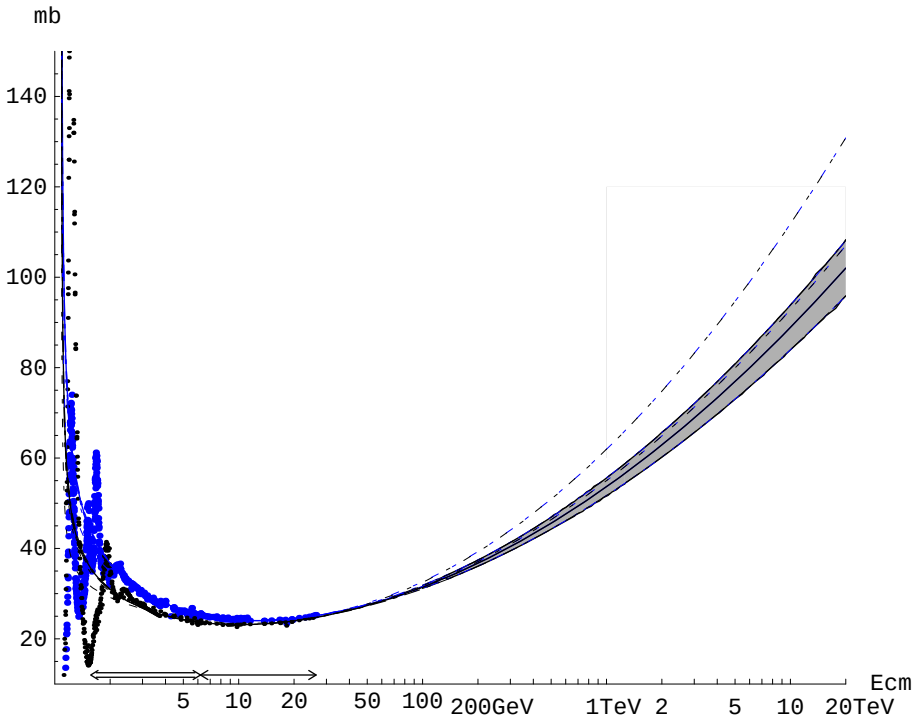


FIG. 5: Prediction of $\sigma_{\rm tot}^{\pi p}$ with the use of FESR in the case $\overline{N_1} = 0.818$GeV as a constraint. The data points are given with no error bars. The big blue points (line) are data (best-fitted curve) for $\pi^- p$. The black points and lines are for $\pi^+ p$. Single horizontal arrow represents the energy region of the fitting, while double horizontal arrow represents the energy region of the FESR integral, $k = \overline{N_1}$ through $\overline{N_2}$(=20GeV). The uncertainty of the prediction by the best fit is shown by shaded region, where $c_2 = (121 \pm 13) \times 10^{-5}$. It is greatly improved from that with no use of FESR, shown by dashed line. The inclusion of rich information of low-energy scattering data through FESR is essential to determine $c_2$.

$\sigma_{\rm tot}^{K^+ p})/2)$ for each value of $\overline{N_1}$ is given in Table II, and the FESR (11) is written in an explicit form. In the case of $\overline{N_1} = 5$GeV, the FESR is given by

$$(Kp) \qquad 8.21363\beta_{P'} + 39.2291 c_0 + 124.142 c_1 + 398.549 c_2 = 38.62 \pm 0.07 \ , \tag{17}$$

which is regarded as a constraint between parameters, $c_{2,1,0}$ and $\beta_{P'}$. Solving this constraint, the $\beta_{P'}$ is represented by the other three parameters. The experimental $\sigma_{\rm tot}^{K^\mp p}$ in $k \geq 20$GeV and $\rho^{K^\mp p}$(more exactly Re $f^{K^\mp p}$) in $k \geq 5$GeV are fitted simultaneously with five parameters, $c_{2,1,0}, \beta_V$ and $F^{(+)}(0)$, where $\alpha_{P'}, \alpha_V$ are fixed with common values to $\pi p$ case, $\alpha_{P'} = 0.5, \alpha_V = 0.497$. The fits are successful, independently of the choices of $\overline{N_1}$, as

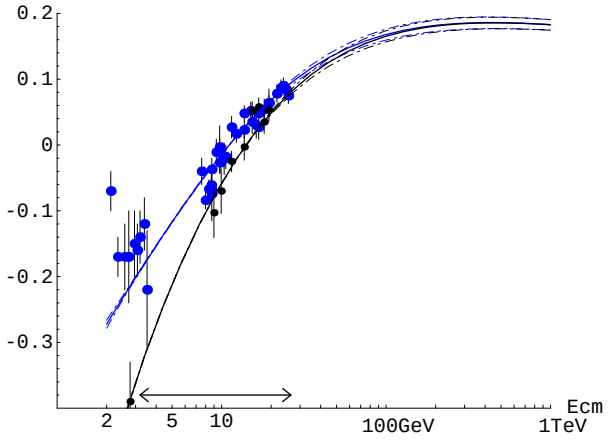


FIG. 6: Result of the fit and prediction of $\rho^{\pi^{\mp}p}$ with the use of FESR in the case $\overline{N_1} = 0.818$GeV as a constraint. The big blue points (line) are data (best-fitted curve) for $\pi^- p$. The black points and lines are for $\pi^+ p$. A horizontal arrow represents the energy region of the fitting.

TABLE VI: Values of $c_2$ and the $\chi^2$ in the best fits to $\sigma_{\rm tot}^{K^{\mp}p}$ and $\rho^{K^{\mp}p}$. The FESR with the integral $\overline{N_1}$ through $\overline{N_2}$ is used as constraints. The $\overline{N_2}$ is fixed to 20GeV while we take various values of $\overline{N_1}$. The number of data points is 111, fitted with 5 parameters in the case with using FESR. The result with no use of FESR is given in the last column as No SR.

| $\overline{N_1}$(GeV) | 10 | 7 | 5 | 4 | 3 | No SR |
|---|---|---|---|---|---|---|
| $c_2(10^{-4})$ | 179(61) | 176(54) | 176(49) | 176(47) | 174(44) | 266(95) |
| $\chi^2_{\rm tot}$ | 64.01 | 63.90 | 63.80 | 63.76 | 63.77 | 62.29 |

shown in Table VI where we only show the values of $c_2$ and the total $\chi^2$ in the best fits.

The central values of $c_2$ in the best fits are very stable, and almost independent of the choices of $\overline{N_1}$. We choose $\overline{N_1} = 5$GeV as a representative of our results. This value is fairly larger than the momentum of the dip structure observed in $\sigma_{\rm tot}^{K^+p}$ below $k \simeq 1.2$GeV. The best-fitted value of $c_2$ is

$$c_2 \;=\; (176 \pm 49) \cdot 10^{-4} \;. \tag{18}$$

The values of the other parameters are given in Table VII. The results are compared with the analysis with no use of FESR,

$$c_2 \;=\; (266 \pm 95) \cdot 10^{-4} \;. \tag{19}$$

TABLE VII: Values of best-fitted parameters and their one-standard deviations in $K^{\mp}p$ scattering. The FESR with $\overline{N_1}$=5GeV is used and $\beta_{P'}$ is obtained from the other parameters by using this FESR. Our predicted lines in Fig. 8 are depicted by using these values.

| $c_2(10^{-4})$ | $c_1$ | $c_0$ | $F^{(+)}(0)$ | $\beta_V$ | $\beta_{P'}$ |
|---|---|---|---|---|---|
| 175.7 | -0.1388 | 1.207 | 1.660 | 0.5684 | 0.1840 |
| +49.5 | -0.2042 | 1.439 | 0.640 | 0.5668 | -0.1775 |
| -49.5 | -0.0733 | 0.974 | 2.680 | 0.5699 | 0.5455 |

This uncertainty of $c_2$ is very large, since the range of momenta of the fitting 20GeV$<$ $k$ $<$310GeV, which corresponds to 6.2GeV$<$ $E_{cm}$ $<$24.1GeV, is insufficient to determine $c_2$ accurately by direct fitting. The value of $\beta_{P'}$ in the best fit becomes negative and unphysical. Thus, the central value $c_2 = 266 \times 10^{-4}$ is considered to be too large and unreliable.

By including the data above $k = 5\text{GeV}(E_{cm} = 3.25\text{GeV})$ in the form of FESR, the error of $c_2$ in Eq. (18) becomes about half of Eq. (19). Correspondingly, the predicted spectra with using FESR given in Fig. 8 are greatly improved from Fig. 7 with no use of FESR. The inclusion of the information in low-energy region is essential to determine the value of $c_2$ reliably in $Kp$ scattering. The fitting results and prediction of $rho^{K^-p,K^+p}$ using FESR are given in Fig. 9.

The figure 2 shows the data in the low-energy region. The low-energy extensions of our best fitted curves in the case of $\overline{N_1}$=5GeV are also depicted in this figure. They reproduce surprisingly well the experimental $\sigma_{\rm tot}^{K^-p}$ and $\sigma_{\rm tot}^{K^+p}$, although the energy region of the FESR integral and the energy region of the fitting are above the energy region shown in this figure. This shows that our best fitted curves satisfy the FESR duality.

### D. Analysis of $\bar{p}p, pp$ scatterings

Similarly to the $Kp$ scatterings, in the analysis of $\bar{p}p, pp$ scatterings we fix $\overline{N_2} = 20\text{GeV}$, while we take various values of $\overline{N_1}$ as $\overline{N_1} = 10, 7, 5, 4, 3\text{GeV}$. For each value of $\overline{N_1}$, the FESR (11) is written in an explicit form, where the integral of $\sigma_{\rm tot}^{(+)}$ $(= (\sigma_{\rm tot}^{\bar{p}p} + \sigma_{\rm tot}^{pp})/2)$ is given in Table III. In the case $\overline{N_1} = 5\text{GeV}$, for example, the FESR is given by

$$(pp) \qquad 3.14058\beta_{P'} + 10.8947c_0 + 27.5046c_1 + 71.0017c_2 = 90.38 \pm 0.20 \ , \tag{20}$$

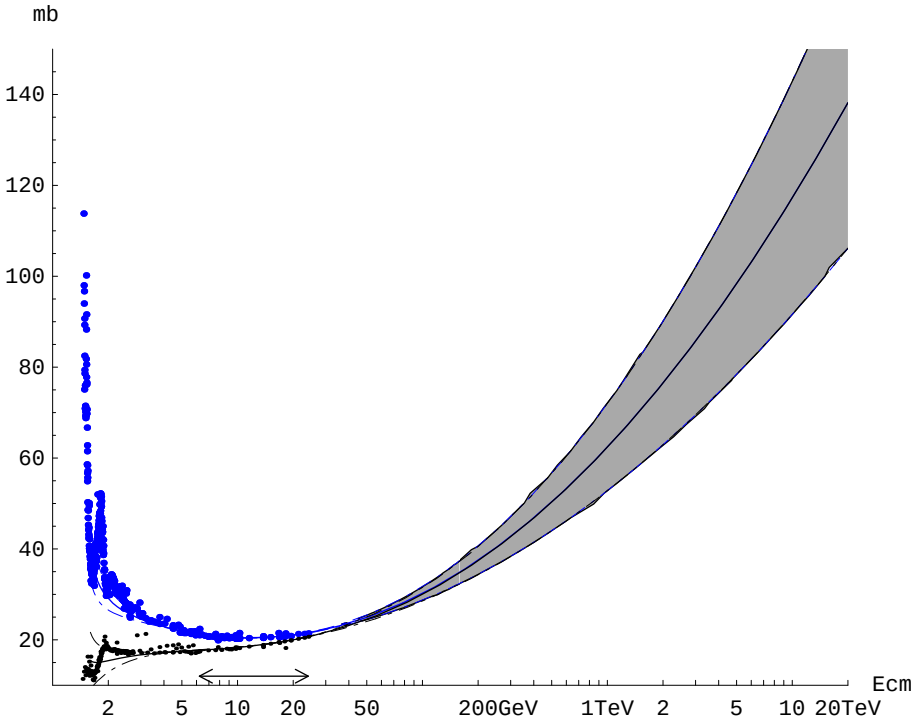


FIG. 7: Prediction of $\sigma_{\rm tot}^{Kp}$ with No use of FESR in The data points are given with no error bars. The big blue points (line) are data (best-fitted curve) for $K^- p$. The black points and lines are for $K^+ p$. The horizontal arrow represents the energy region of the fitted data. The shaded region represents the uncertainty of the prediction, where $c_2 = (266 \pm 95) \times 10^{-4}$. The $c_2$ has a very large uncertainty since it is not determined well by direct fitting to the high-energy experimental data.

which is regarded as a constraint between parameters, $c_{2,1,0}$ and $\beta_{P'}$, and leads to the relation $\beta_{P'} = \beta_{P'}(c_2, c_1, c_0)$.

The $\sigma_{\rm tot}^{\bar{p}p}$ data are obtained up to $E_{cm} = 63$GeV by ISR experiment, up to $E_{cm} = 0.9$TeV by SPS experiment, and up to $E_{cm} = 1.8$TeV by Tevatron experiment. There are two conflicting measurements in Tevatron experiment, by D0[23, 24] and CDF[25]. The very high-enegy data with large uncertainties are obtained by cosmic ray experiments.

The experimental $\sigma_{\rm tot}^{\bar{p}p,pp}$ in $k \geq 20$GeV and $\rho^{\bar{p}p,pp}$ in $k \geq 5$GeV, up to Tevatron energy, are fitted simultaneously. The fittings are performed with five parameters, $c_{2,1,0}, \beta_V$ and $F^{(+)}(0)$, by using FESR as a constraint[44]. The best fitted values of $c_2$ and total $\chi^2$ for the respective values of $\overline{N_1}$ are given in Table VIII. The result is compared with the six-parameter fit of the analysis without using FESR, denoted as No SR in the same table. By considering this result, we choose $\overline{N_1} = 5$GeV as a representative of our analyses. The best-fitted $c_2$ is given

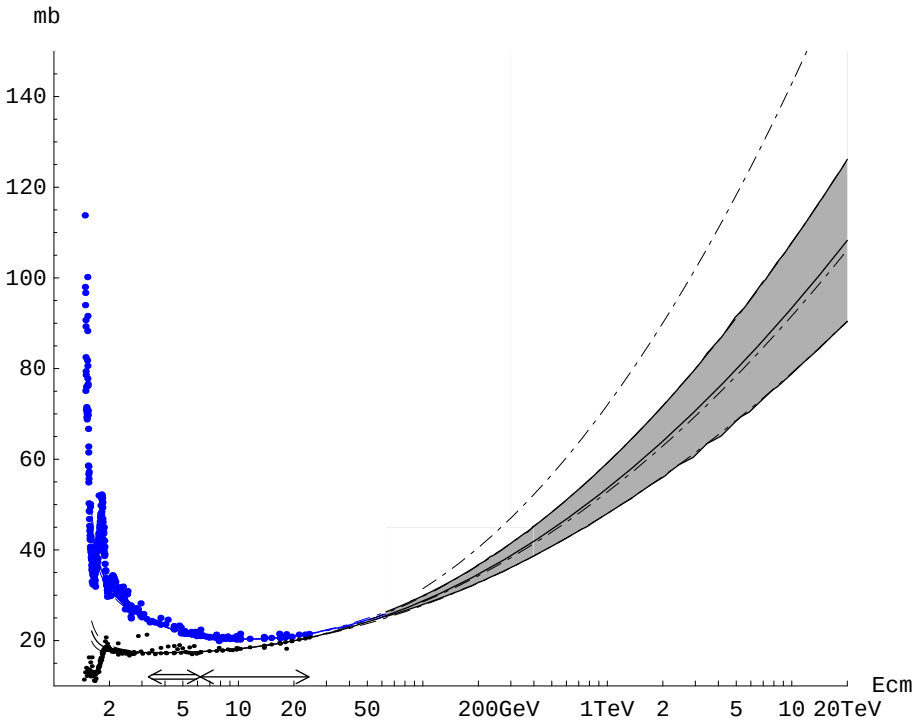


FIG. 8: Prediction of $\sigma_{\rm tot}^{Kp}$ with using FESR in the case $\overline{N_1}$ = 5GeV as a constraint: The big blue points (line) are data (best-fitted curve) for $K^-p$. The black points and lines are for $K^+p$. Single horizontal arrow represents the energy region of the fitted data, while double horizontal arrow represents the energy region of the FESR integral, $k = \overline{N_1}$ through $\overline{N_2}$(=20GeV). The data points are given with no error bars. The uncertainty of the prediction by the best fit, shown by shaded region, is improved from that with no use of FESR, represented by dot-dashed line. The best-fitted $c_2$ is $c_2 = (176 \pm 49) \times 10^{-4}$. The inclusion of the information of low-energy data by FESR is essential to improve the estimation of $c_2$.

by

$$c_2 \;=\; (504 \pm 26) \cdot 10^{-4} \;. \tag{21}$$

The values of the other parameters are given in Table IX.

The improvement from the result $c_2 = (491 \pm 34) \cdot 10^{-4}$ obtained by the fit without using FESR is not large, since the high-energy data by SPS and Tevatron experiments, which affects directly the estimation of $c_2$-value, are included in both fits.

Our predicted spectra of $\sigma_{\rm tot}^{\bar{p}p,pp}$ in the case of $\overline{N_1}$=5GeV are given in Fig. 10. Fitting result and prediction of $\rho^{\bar{p}p,pp}$ are given in Fig. 11.

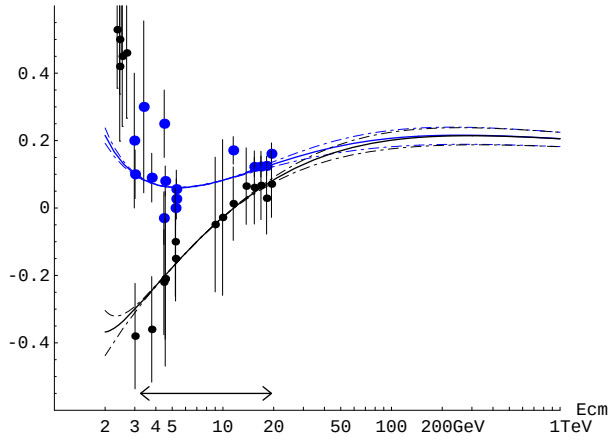


FIG. 9: Result of the fit and prediction of $\rho^{K^{\mp}p}$ with the use of FESR in the case $\overline{N_1} = 5$GeV as a constraint. The big blue points (line) are data (best-fitted curve) for $K^-p$. The black points and lines are for $K^+p$. A horizontal arrow represents the energy region of the fitting.

TABLE VIII: Values of $c_2$ and the total $\chi^2$ in the best fit to $\bar{p}p, pp$ scatterings, using FESR as a constraint. The data up to Tevatron energy, $E_{cm} = 1.8$TeV, are fitted simultaneously. The number of data points is 234, fitted by 5 parameters in the case using FESR as a constraint. The result of six-parameter fit without using FESR is also shown in the last column as No SR.

| $\overline{N_1}$ | 10 | 7 | 5 | 4 | 3 | No SR |
|---|---|---|---|---|---|---|
| $c_2(10^{-4})$ | 505(28) | 506(27) | 504(26) | 500(26) | 493(25) | 491(34) |
| $\chi^2_{\rm tot}$ | 214.52 | 214.53 | 214.32 | 214.14 | 213.99 | 213.98 |

### E. Test of the universality of $B$

Using the values of parameters given in the previous subsections, we can test the universality of $B$ parameters from the experimental data of $\pi^{\mp}p$, $K^{\mp}p$ and $\bar{p}(p)p$ scatterings.

In ref.[6] the asymptotic formula of total cross section is represented in terms of squared CM energy $s$ in the form

$$\sigma_{\rm tot}^{(+)} \simeq Z^{ap} + B \log^2 \frac{s}{s_0} , \tag{22}$$

which is already given in Eq. (3). In ref.[6] $B$ and $s_0$ is assumed to be universal in the relevant processes while $Z_{ap}$ are taken to be process-dependent[45].

TABLE IX: Values of best-fitted parameters and their one-standard deviations in $\bar{p}p, pp$ scattering. The FESR with $\overline{N_1}$=5GeV is used and $\beta_{P'}$ is obtained from the other parameters by using this FESR. Our predicted lines in Figs. 10 and 11 are depicted by using these values.

| $c_2(10^{-4})$ | $c_1$ | $c_0$ | $F^{(+)}(0)$ | $\beta_V$ | $\beta_{P'}$ |
|---|---|---|---|---|---|
| 503.6 | -0.2432 | 6.647 | 10.51 | 3.721 | 6.713 |
| +26.1 | -0.2810 | 6.788 | 10.24 | 3.728 | 6.495 |
| −26.1 | -0.2054 | 6.505 | 10.77 | 3.714 | 6.931 |

We use the asymptotic formula of crossing-even amplitude (6) which gives

$$\sigma_{\rm tot}^{(+)} \simeq \frac{4\pi}{m^2}\left(c_0 + c_1 \log\frac{\nu}{m} + c_2 \log^2\frac{\nu}{m}\right) . \tag{23}$$

It is the same equation as Eq. (2). Here we omit the $P'$-term proportional to $\beta_{P'}$ and use the approximation $\nu/k \simeq 1$ in high energies.

Using the relation $s \simeq 2M\nu$ at high-energies from Eq. (1), we obtain the relation between the parameters

$$B = \frac{4\pi}{m^2} c_2 , \tag{24}$$

$$Z^{ap} = \frac{4\pi}{m^2}\left(c_0 - \frac{{c_1}^2}{4c_2}\right) , \tag{25}$$

$$s_0 = 2Mm \exp\left[-\frac{c_1}{2c_2}\right] + M^2 + m^2 . \tag{26}$$

The parameters $c_{2,1,0}$ are treated as process-dependent in our analyses. Substituting the best-fitted values of $c_{2,1,0}$ into these equations, we can estimate the values of $B, Z^{ap}, \sqrt{s_0}$ individually for $\pi p, Kp$ and $\bar{p}p, pp$ scatterings without using the universality hypothesis. The results are given in Table X. The results with using FESR are given in the LHS, and those without using FESR are given in the RHS.

As shown in this table, in the case of using FESR, the values of $B$ for $\pi p, Kp$ and $\bar{p}(p)p$ scatterings denoted, respectively, as $B_{\pi p}, B_{Kp}$ and $B_{pp}$, are mutually consistent within one standard deviation.

In contrast, if we do not use the FESR as constraints, $B_{\pi p}$ and $B_{Kp}$ have large uncertainties, and we cannot obtain any definite conclusion.

It is very interesting that by including rich informations of low-energy scattering data through FESR, the central values of $B$ become mutually closer, and consistent with each

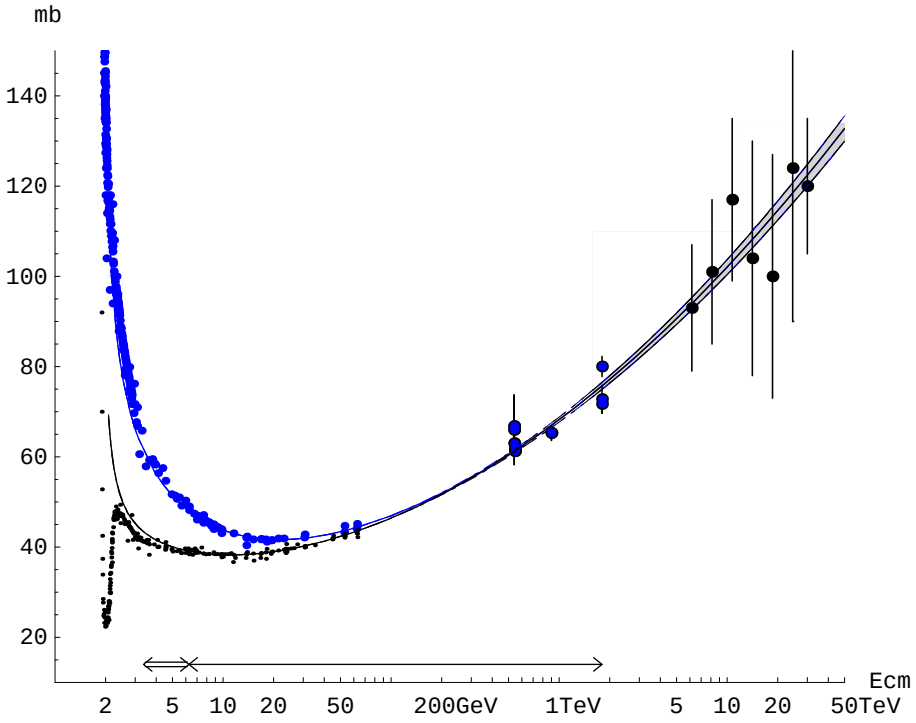


FIG. 10: Prediction of $\sigma_{\rm tot}^{\bar{p}p,pp}$ with using FESR: The data up to Tevatron energy are fitted simultaneously. The single horizontal arrow represents the energy region of the fitting. The big blue points (line) are data (best-fitted curve) for $\bar{p}p$. The black points and lines are for $pp$. The data points are given with no error bars. The double horizontal arrow represents the energy region of the FESR integral, $k$=$\overline{N_1}$(=5GeV in this case) through $\overline{N_2}$(=20GeV). The shaded region corresponds to the uncertainty of our prediction in the best fit, where $c_2 = (504 \pm 26) \times 10^{-4}$.

other. The FESR duality suggests the universality of $B$.

Another interesting feature is the values of $Z^{ap}$. If we neglect relatively small contributions from $\beta_{P'}$ and $\beta_V$ terms the $Z^{ap}$ are equal to the $\sigma_{\rm tot}$ at energy $\sqrt{s_0}$, which is the lowest point of parabola (23) of $\log\frac{\nu}{m}$. The values of $Z^{ap}$ for $\pi p, Kp$ and $\bar{p}(p)p$ approximately satisfy the relation of the quark model $Z^{\pi p} : Z^{Kp} : Z^{pp} \simeq 2 : 2 : 3$. $Z^{ap}$ and the parameters $\beta_{P'}$ and $\beta_V$ appearing in the Regge theory are controlled by non-perturbative soft physics of QCD, while the term $B \log^2 s/s_0$ describing the rise of $\sigma_{\rm tot}$ is plausibly universal for hadron-hadron scatterings.

It is to be noted that this picture is inferred in an early work[9] where it is stated that "the first, constant term[corresponding to $Z^{ap}$ in Eq. (22) in the present article] ... corresponds to a process-dependent(valence quark scattering) contribution, whereas the second, logarith-

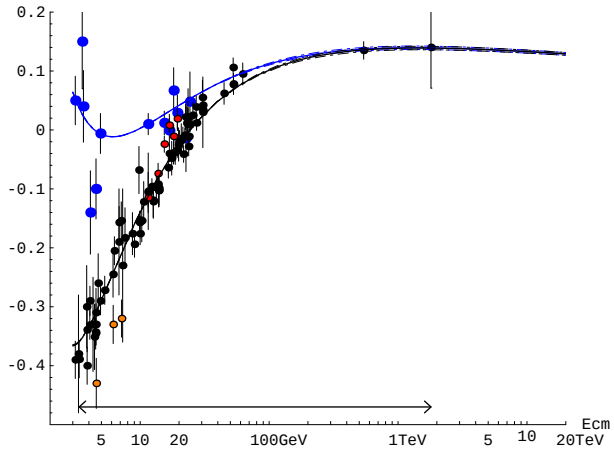


FIG. 11: Result of the fit and prediction of $\rho^{\bar{p}p,pp}$ with the use of FESR in the case $\overline{N_1} = 5$GeV as a constraint. The big blue points (line) are data (best-fitted curve) for $\bar{p}p$. The black points and lines are for $pp$. A horizontal arrow represents the energy region of the fitting. $\rho^{pp}$ data by ref.[26](red points) and by ref.[27](orange points) are removed from our best fit.

TABLE X: Values of $B$, $Z^{ap}$ and $\sqrt{s_0}$ obtained from our best fits with using FESR(LHS) and without using FESR (RHS). The $B$, $Z^{ap}$ and $\sqrt{s_0}$ are estimated individually for the processes of $\pi p$, $Kp$ and $\bar{p}(p)p$ scatterings.

| | $B$(mb) | $Z^{ap}$(mb) | $\sqrt{s_0}$(GeV) | $B$(mb) | $Z^{ap}$(mb) | $\sqrt{s_0}$(GeV) |
|---|---|---|---|---|---|---|
| $\pi p$ | 0.304(34) | 21.45(32) | 5.92(90) | 0.411(73) | 22.99 | 9.71 |
| $Kp$ | 0.354(99) | 18.7(1.1) | 7.1(2.6) | 0.535(190) | 20.67 | 12.14 |
| $\bar{p}(p)p$ | 0.280(15) | 35.31(36) | 4.63(53) | 0.273(19) | 34.98 | 4.28 |

mically rising one is universal (gluon scattering)." "We conclude that it is the FNAL(-ISR) energy interval where $\sigma^{MB}/\sigma^{BB}$(the ratio of the $\sigma_{\rm tot}$ for meson-baryon scattering to the baryon-baryon scattering) comes closest to 2/3. With the further increase of energy the ratio will approach unity."

In the arguments of color glass condensate(CGC) of QCD, the gluon component of the target particle drastically increases in high-energy scattering. This is based on the calculation of perturbative QCD. The radius $R$ of the "black" region where strong absorption of incident particles occurs increases plausibly by a log $s$ term with a universal coefficient. The $\sigma_{\rm tot}$ may be given by $2\pi R^2$ and the factor $B$ is expected to be universal for $\pi p, Kp$ and

$\bar{p}p, pp$.

In ref.[6] the $s_0$ as well as $B$ are taken to be universal in the fittings. The $\sqrt{s_0}$ is not suggested to be process-independent both in ref.[9] and in the framework of CGC. In Table X the values of $\sqrt{s_0}$ for the relevant three processes seem to be closer to each other in the case of using FESR, compared with the case of no use of FESR. This possibility will be investigated in the next subsection.

### F. Analysis with common value of $B$

Our analyses in previous subsections suggest the universality of $B$ in $\pi p$, $Kp$ and $\bar{p}(p)p$ scatterings. Now let us try to fit all the data by taking the same value of $B$ from the beginning. The $\sigma_{\rm tot}$ above $k \geq 20$GeV and $\rho$ above $k \geq 5$GeV for $\pi^{\mp}p, K^{\mp}p, \bar{p}(p)p$ scatterings are fitted simultaneously. There are three sets of parameters, $c_2, c_1, c_0, F^{(+)}(0), \beta_{P'}, \beta_V$. The three FESR (14),(17) and (20) are used as constraints. Now three $c_2$ are not independent. They are represented by one universal $B$ parameter through Eq. (24). So the number of fitting parameters is 13. Successful fits are obtained with the total $\chi^2 = 429.55 = 150.83(\pi^{\mp}p) + 64.28(K^{\mp}p) + 214.44(\bar{p}(p)p)$ with $(N_D - N_P) = (508 - 13)$. It is compared with the best fitted $\chi^2$ for respective data sets with no universality constraints, which are given in the tables IV, VI and VIII: $\chi^2/(N_D - N_P) = 150.51/(162-5)$ for $\pi^{\mp}p$, $63.80/(111-5)$ for $K^{\mp}p$, $214.32/(235-5)$ for $\bar{p}(p)p$. Their sum is 428.62. The increase of total $\chi^2$ is, thus, only 0.93. The constraint of universal $B$ is consistent with the present experimental data.

The value of $B$ in this universality fit is given by

$$B \ = \ 0.285 \pm 0.013 \text{ mb}. \tag{27}$$

The values of $\sqrt{s_0}$ and $Z^{ap}$ are also given in the upper half of Table XI.

By taking the value of $B$ to be universal, the best-fitted values of $\sqrt{s}_0$ become closer to each other. Successful fits are obtained in ref.[6] by taking both $B$ and $s_0$ being universal. We also try to fit the data by taking both $B$ and $s_0$ being common in the relevant three processes. The resulting $\chi^2 = 435.24 = 152.19(\pi^{\mp}p) + 64.06(K^{\mp}p) + 219.00(\bar{p}(p)p)$ with 11 parameters, and the fit is successful. The increase of $\chi^2$ is totally 6.62 from the best fits to respective processes with no constraints of $B$ and $s_0$.

The values of parameters are given in the lower half of Table XI. The $B$ and $\sqrt{s_0}$ are

TABLE XI: Values of parameter in the best fits by assuming universality of $B$ and of $B$ and $s_0$, which are taken to be common in fitting the data of relevant processes. The $B$, $Z^{ap}$ and $\sqrt{s}_0$ are related with $c_2, c_0$ and $c_1$ by Eqs. (24), (25) and (26). The $\beta_{P'}$ are obtained from values of the other parameters through FESR.

| | $B$(mb) | $\sqrt{s_0}$(GeV) | $Z^{ap}$(mb) | $F^{(+)}(0)$ | $\beta_V$ | $\beta_{P'}$ |
|---|---|---|---|---|---|---|
| $\pi p$ | 0.285(13) | 5.40(37) | 21.24(16) | 0.13(61) | 0.04012(95) | 0.1527(62) |
| $Kp$ | 0.285(13) | 5.17(38) | 17.91(19) | 2.33(1.01) | 0.5618(82) | 0.4296(481) |
| $\bar{p}(p)p$ | 0.285(13) | 4.82(49) | 35.44(32) | 10.41(60) | 3.723(36) | 6.637(198) |
| $\pi p$ | 0.304(10) | 5.75(34) | 21.36(15) | -0.10(61) | 0.04043(93) | 0.1472(61) |
| $Kp$ | 0.304(10) | 5.75(34) | 18.19(16) | 2.11(1.01) | 0.5613(81) | 0.3535(461) |
| $\bar{p}(p)p$ | 0.304(10) | 5.75(34) | 36.04(17) | 9.88(53) | 3.745(35) | 6.232(122) |

given by $B = 0.304 \pm 0.010$mb and $\sqrt{s_0} = 5.75 \pm 0.34$GeV. These values are consistent with the results given in PDG[6], $B = 0.308(10)$mb and $\sqrt{s_0}$=5.38(50)GeV, which are obtained by assuming the universality of $B$ and $s_0$. Another interesting feature is the ratio of $Z^{ap}$. It satisfies approximately the quark model prediction, $Z^{\pi p} : Z^{Kp} : Z^{pp} = 2 : 2 : 3$.

## V. CONCLUDING REMARKS

In order to test the universal rise of total cross section $\sigma_{\rm tot}^{(+)}$ by $\log^2 s/s_0$ in all the hadron-hadron scatterings, we analyze $\pi^{\mp}p$, $K^{\mp}p$ and $\bar{p}(p)p$ scatterings independently. Rich information of low-energy scattering data constrain, through FESR, the parameters in high-energy asymptotic formula to fit experimental $\sigma_{\rm tot}$ and $\rho$ ratios. The values of $B$ parameters, the coefficients of $\log^2 s/s_0$ term in $\sigma_{\rm tot}^{(+)}$, are obtained individually for three processes by these analyses. The results are given in the LHS of Table X, which is explicitly shown in Fig. 12. We obtain

$$B_{\pi p} \simeq B_{Kp} \simeq B_{pp} \quad . \tag{28}$$

The results are consistent with the universality of $B$ within one standard deviation. The universality of $B$ is suggested in our analyses.

There are several remarks in our results.

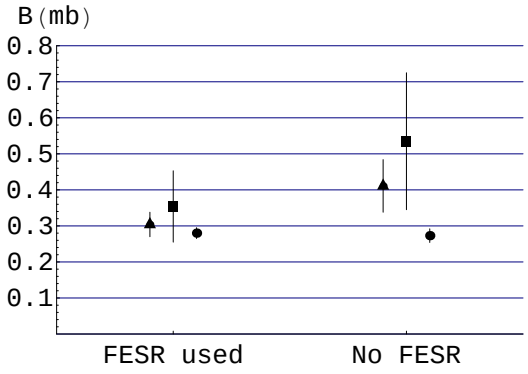


FIG. 12: Values of $B$ parameters in Table X: Results with No use of FESR(RHS) and ones with using FESR (LHS). Triangles, squares and circles represent $B_{\pi p}$, $B_{Kp}$ and $B_{pp}$, respectively. Errors represent one standard($1\sigma$) deviations. $B_{\pi p} = B_{Kp} = B_{pp}$ is satsified within $1\sigma$ in the case using FESR, while we do not obtain any definite conclusion in the case with no use of FESR.

**i)** In order to obtain the above conclusion it is essential to use the FESR as constraints between fitting parameters. As shown in RHS of Fig. 12, if we do not use the FESR, $B_{\pi p}$ and $B_{Kp}$ cannot be estimated with sufficient accuracy, and we could not obatin any definite conslusion.

**ii)** The absolute magnitude of $B$ in the best fit is dependent fairly largely upon the energy region of the fittng in the present $\bar{p}p$ scattering data. In the fit to all the data up to Tevatron energy $\sqrt{s} = 1.8$TeV, the $B_{pp}$ is estimated as $B_{pp} = 0.280 \pm 0.015$mb, which predicts the $\sigma_{\rm tot}^{pp} = 108.0 \pm 1.9$mb at the LHC energy $\sqrt{s} = 14$TeV. While if only the data up to the ISR energy $\sqrt{s} = 63$GeV are taken into account, we obtain $B_{pp} = 0.317 \pm 0.034$mb, which predicts $\sigma_{\rm tot}^{pp} = 113.2 \pm 4.6$mb at LHC energy. This value is consistent with the above prediction, but its central value is somewhat larger than our previous result[3, 17]. The precise measurement of $\sigma_{\rm tot}^{pp}$ in LHC[13, 14] will help to fix the uncertainty of the absolute magnitude of $B$.

**iii)** Our approach can be checked by the measurement of $\sigma_{\rm tot}^{pp}$ in LHC. Our predicted values of $\sigma_{\rm tot}^{pp}$ and $\rho^{pp}$ at LHC $\sqrt{s} = 14$TeV as well as the other predictions [39] are given in Table XII for comparison. The predictions in various models have a wide range. The LHC will select among these approaches.

**iv)** The best fitted values of $B_{\pi p}$ and $B_{Kp}$ are almost the same with each other. This result

| ref. | $\sigma_{\rm tot}^{pp}$(mb) | $\rho^{pp}$ |
|---|---|---|
| II[this work] | 108.0±1.9 | 0.1312±0.0024 |
| II[3] | $106.3\pm5.1_{\rm syst}\pm2.4_{\rm stat}$ | $0.126\pm0.007_{\rm syst}\pm0.004_{\rm stat}$ |
| BH[4] | 107.3±1.2 | 0.132±0.001 |
| BSW[28] | 103.6 | 0.122 |
| GLMM[29, 30] | 92.1, 110.5 | |
| RMK[31] | 91.7 | |
| COMPETE[32] | $111.5\pm1.2_{\rm syst}\ ^{+4.1}_{-2.1{\rm stat}}$ | $0.1361\pm0.0015_{\rm syst}\ ^{+0.0058}_{-0.0025{\rm stat}}$ |
| MN[33] | 106.4 | 0.127 |
| GKS[34] | 128 | 0.19 |
| CS[35] | 152 | 0.26 |
| PP[36] | $106.73^{+7.56}_{-8.50}$ | $0.1378^{+0.0042}_{-0.0612}$ |
| ILP[37] | 110 | 0.12 |
| Landshoff[38] | 125±25 | |

TABLE XII: Predictions of $\sigma_{\rm tot}^{pp}$ and $\rho^{pp}$ at LHC $\sqrt{s} = 14$TeV in various models.

is important since it suggests the value of $B$ is independent of quark flavors. The $B_{\pi p}$ is also consistent with $B_{pp}$. Thus, we expect the universality of $\sigma_{\rm meson-baryon} \simeq \sigma_{\rm baryon-baryon}$ independently of quark flavors in super high energies, as was suggested in refs.[9, 10, 11]. In order to establish the universality of $B$ for all the hadronic scatterings it is also important to analyze the other processes, such as $\Sigma^- p$ and $\Lambda p$ scatterings.

**v)** If the universality of $B$ is estalished both theoretically and experimentally, the total cross sections of all the hadronic scatterings are described simply by Eq. (3), $\sigma_{\rm tot} \simeq B\ \log^2 s/s_0 + Z^{ap}$, for $\sqrt{s} > \ \sim\sqrt{s_0} \simeq 5$GeV, where the effects from Regge poles of $P'$ and of vector trajectory become negligible. $B$ is a universal constant. There is an interesting possibility that $\sqrt{s_0}$ is universal. There is no way of predicting values of $Z^{ap}$, which are highly non-perturbative object. Difference between $Z^{\pi p}$ and $Z^{Kp}$ is not large, about 3mb, and the $Z^{\pi p}$, $Z^{Kp}$ and $Z^{pp}$ approximately satisfy the ratio $2:2:3$, predicted by quark model.

[1] K. Igi, M. Ishida, Phys. Rev. D **66**, 034023 (2002).

[2] J.R.Cudell et al. ( COMPETE Collab.), Phys. Rev. D **65**, 074024 (2002).

[3] K. Igi, M. Ishida, Phys. Lett. B **622**, 286 (2005).

[4] M. M. Block, F. Halzen, Phys.Rev. D **72**, 036006 (2005) [Errata; **72**, 039902 (2005)].

[5] M. Ishida and K. Igi, Phys. Lett. B **670**, 395 (2009).

[6] Particle Data Group, W.-M. Yao et al., J. Phys. G: Nucl. Part. Phys. **33**, 337 (2006).

[7] M. Froissart, Phys. Rev. **123**, 1053 (1961).

[8] A. Martin, Nuovo Cimento **42**, 930 (1966).

[9] L. L. Jenkovszky, B. V. Struminsky and A. N. Wall, Yad. Fiz. **46**, 1519 (1987). 'Where is "asymptopia"?',1986, ITP-86-82E.

[10] E. Ferreiro, E. Iancu, K. Itakura, L. McLerran, Nucl. Phys. A **710**, 373 (2002).

[11] L. Frankfurt, M. Strikman, M. Zhalov, Phys. Lett. B **616**, 59 (2005).

[12] E. Iancu, A. Leonidov, L. McLerran, Nucl. Phys. A **692**, 583 (2001); Phys. Lett. B **510**, 133 (2001).

[13] TOTEM: Technical Design Reprrt, CERN-LHCC-2004-002; addendum CERN-LHCC-2004-020.

[14] ALFA: ALFA detector: Technical Design Report, ATLAS Forward Detectors for Measurement of Elastic Scattering and Luminosity, ATLAS-TDR-018, CERN-LHCC-2008-004.

[15] SELEX collaboration, U. Dersch et al., Nucl. Phys. B **579**, 277 (2000).

[16] M. Ishida , K. Igi, Eur. Phys. J. C **52**, 357 (2007).

[17] K. Igi, M. Ishida, Prog. Theor. Phys. **116**, 1097 (2006).

[18] K. Igi, Phys. Rev. Lett. **9**, 76 (1962).

[19] K. Igi, S. Matsuda, Phys. Rev. Lett. **18**, 625 (1967).

[20] R. Dolen, D. Horn, C. Schmid, Phys. Rev. **166**, 1768 (1968).

[21] F. J. Gilman, H. Harari, Y. Zarmi, Phys. Rev. Lett. **21**, 323 (1968).

[22] M. M. Block, Nucl. Instrum. Methods A **556**, 308 (2006).

[23] E710 collaboration, N. A. Amos et al., Phys. Rev. Lett. **68**, 2433 (1992).

[24] E811 collaboration, C. Avila et al., Phys. Lett. B**445**, 419 (1999).

[25] CDF collaboration, F. Abe et al., Phys. Rev. D**50**, 5550 (1994).

[26] L. A. Fajardo et al., Phys. Rev. D **24**, 46 (1981).

[27] G. Bellettini et al., Phys. Lett. **14**, 164 (1965).

[28] C. Bourrely, J. Soffer and T. T. Wu, Nucl. Phys. B **247**, 15 (1984).

[29] E. Gotsman, E. Levin, U. Maor and J. S. Miller, arXiv:0805.2799[hep-ph], Eur. Phys. J. C **57**, 689 (2008).

[30] E. Gotsman, E. Levin and U. Maor, arXiv:0708.1506[hep-ph],

[31] M. G. Ryskin, A. O. Martin and V. A. Khoze, arXiv:0812.2407[hep-ph], Eur. Phys. J. C **60**, 249 (2009).

[32] J. R. Cudell et al., [COMPETE collaboration], Phys. Rev. Lett. **89**, 201801 (2002).

[33] E. Martynov and B. Nicolescu, arXiv:0712.1685[hep-ph], Eur. Phys. J. C **56**, 57 (2008).

[34] S. V. Goloskokov, S. P. Kuleshov and O. V. Selyugin, Part. and Nucl. **18**, 39 (1987); Z. Phys. C **50**, 455 (1991).

[35] J. R. Cudell and O. V. Selyugin, hep-ph/0612046, Phys. Lett. B **662**, 417 (2008).

[36] V. A. Petrov and A. Prokudin, hep-ph/0105209, Eur. Phys. J. C **23**, 135 (2002).

[37] M. M. Islam, R. J. Luddy and A. V. Prokudin, Phys. Lett. B **605**, 115 (2005).

[38] P. V.Landshoff, "The Total cross-section at the LHC," Lectures at School on QCD, Calabria. July 2007, hep-ph/0709.0395.

[39] R. Fiore, L. Jenkovszky, R. Orava, E. Predazzi, A. Prokudin, and O. Selyugin, arXiv:0810.2902v2[hep-ph],

[40] In p.337 of ref.[6] $\sigma_{\rm tot}^{\bar{a}p,ap}$ is given by $\sigma_{\rm tot}^{\bar{a}p,ap} = Z^{ap} + B\ \log^2\frac{s}{s_0} + Y_1^{ap}(\frac{s_1}{s})^{\eta_1} \pm Y_2^{ap}(\frac{s_1}{s})^{\eta_2}$. The scale $s_1$ is fixed to be $1{\rm GeV}^2$. The $(B,\ \sqrt{s_0},\ \eta_1,\ \eta_2) = (0.308(10){\rm mb},\ 5.38(50){\rm GeV},\ 0.458(17),\ 0.545(7))$ obtained process-independently. The process-dependent parameters $(Z^{ap},\ Y_1^{ap},\ Y_2^{ap})$ are obtained as (20.86(40), 19.24(1.22), 6.03(19)), (17.91(36), 7.1(1.5), 13.45(40)) and (35.45(48), 42.53(1.35), 33.34(1.04)) for $\pi^{\mp}p$, $K^{\mp}p$ and $\bar{p}(p)p$, respectively. We made Im $f_{\rm PDG}^{\bar{a}p,ap}(\nu)$ by $\frac{k}{4\pi}\times\sigma_{\rm tot}^{\bar{a}p,ap}$ with the central values of these parameters. Multiplying Im $f_{\rm PDG}^{\bar{a}p,ap}(\nu)$ with the $\rho^{\bar{a}p,ap}$ data at the corresponding energies we obatin the data of Re $f^{\bar{a}p,ap}$ . Here we omit errors of $\sigma_{\rm tot}^{\bar{a}p,ap}$ since errors of $\rho^{\bar{a}p,ap}$ are generally larger than $\sigma_{\rm tot}^{\bar{a}p,ap}$.

[41] The following data points are removed: $(k({\rm GeV}),\sigma_{\rm tot}^{\bar{p}p}({\rm mb}))= (2.5, 79.4\pm 1.0), (3.54, 69.7\pm 0.5), (3.6, 76.2\pm 1.8), (4., 71.\pm 1.), (4.015, 66.84\pm 0.32), (4.3, 60.6\pm 0.8), (9.14, 57.51\pm 0.73)$. This procedure is explained in ref.[17].

[42] The $\chi^2$=48.8 for sieved $\bar{p}p$ data includes the factor $R = 1.140$. See ref.[22].

[43] We adopt a different treatment of data from ref.[5], where systematic errors were taken to be larger than those in the original ones[6].

[44] The original data of $\rho^{pp}$ gives no successful fits, since the data are mutually inconsistent with different experiments. Data points by refs.[26] and [27] have comparatively small errors, and seem to be inconsistent with the other data sets by inspection. We have tried to fit the data set only including [26] for $\rho^{pp}$ in the relevant energy region, but it is not successful. We remove these two data sets from our best fit.

[45] Ref.[6] treat the scatterings of $\bar{p}(p)p, \bar{p}(p)n, \Sigma^- p, \pi^{\mp} p, K^{\mp} p, K^{\mp} n, \gamma p, \gamma\gamma$. All data sets are fitted by using a common value of $B$ (and a common value of $s_0$). The resulting $B$ is $B = 0.308(10)$mb.